Istraživanja i projektovanja za privredu
ISSN 1451-4117
DOI:10.5937/jaes0-72517
www.engineeringscience.rs

iipp publishing

Journal of Applied Engineering Science
Original Scientific Paper,
Volume 24, Number 4, Year 2026,
no 1376, pp 851-861

WET STRAINING FIBRE ALIGNMENT AS AN ADDITIVE-FREE STRATEGY FOR INCREASING MECHANICAL PERFORMANCE OF RECYCLED PAPER

Gigih Laksana Dewanda[1], Ubaidillah[1]*, Siti Amalina Azahra[2], Joanne Li[3], Mujtahid Kaavessina[4], Dharu Feby Smaradhana[1]*

[1]Sebelas Maret University, Faculty of Engineering, Department of Mechanical Engineering, Surakarta, Indonesia
[2]National Research and Innovation Agency (BRIN), Research Center for Advanced Materials, South Tangerang, Banten, Indonesia
[3]Imperial College London, Faculty of Engineering, Department of Aeronautics, London, United Kingdom
[4]Sebelas Maret University, Faculty of Engineering, Department of Chemical Engineering, Surakarta, Indonesia
**ubaidillah_ft@staff.uns.ac.id* **dharufs@staff.uns.ac.id*

Hornification reduced the bonding ability of recycled cellulose fibres and limited the strength of recycled paper. This study examined fibre alignment through wet straining (WS) as an additive-free strategy to increase the strength of recycled paper. The route comprised wet sheet forming from used paper, uniaxial straining at a low strain rate and hot pressing, without virgin fibres or chemical additives. Tensile and single-edge-notched tension (SENT) tests compared specimens cut parallel (WS 0) and perpendicular (WS 90) to the straining direction with unstrained sheets (No straining). Wet straining produced a moderate dominant fibre direction along the straining axis. Grammage and porosity did not differ significantly among the groups. Densification was therefore an unlikely cause of the mechanical differences. WS 0 had a tensile modulus of 0.87 GPa and a tensile strength of 10.15 MPa. These values were 142% and 22% higher than those of No straining (0.36 GPa and 8.34 MPa, respectively). The mean tensile modulus and tensile strength of WS 90 were smaller than those of No straining. These differences were not significant. Fracture resistance improved more than tensile strength. WS 0 had an apparent fracture toughness (Kmax) of 1.51 MPa m0.5. This value was 82% higher than that of No straining (0.83 MPa m0.5). Wet straining therefore increased the stiffness, strength and fracture resistance of recycled paper along the straining direction. Fibre orientation can thus serve as an additive-free design parameter for upgrading recycled fibrous materials in a circular economy, with potential relevance to printing grades.

Keywords: fibre alignment, wet straining, fracture toughness, recycled cellulose fibres

HIGHLIGHTS

- Wet straining orients hornified recycled paper fibres to a moderate degree without virgin fibres or chemical additives.
- Similar grammage and porosity make densification an unlikely cause of the mechanical differences between groups.
- Tensile strength is significantly higher along the straining axis than in unstrained recycled paper.
- Apparent fracture toughness (Kmax) rises by 82% over unstrained paper, probably owing to crack bridging by fibres.

1 Introduction

Paper is one of the most widely circulated materials in the world. Global production of paper and paperboard reached 417 million tonnes in 2022, of which ~244 million tonnes (~58%) originated from recycled fibres [1]. Recycling rates vary across regions. In the United States, the recycling rate for all paper grades has been reported at 67.9% [2]. Nevertheless, part of the waste paper is still disposed of in landfills, where anaerobic decomposition can generate methane, a greenhouse gas [2]. The supply chain is also vulnerable to global trade policies. After China imposed waste import bans that culminated in the National Sword policy, US exports of recovered paper fell to 14.3 million tonnes in 2020 [3]. Trade patterns have also shifted, as have the availability and quality of secondary fibres on the international market [2]. Moreover, each cycle of repulping, de-inking, and drying causes fibre shortening, hornification, hemicellulose loss, and reduced bonding ability. Consequently, fibres can be recycled only ~5 to 7 times [2]. The tensile strength of chemical pulp has also been reported to decrease by 10–70% after recycling [1]. Fibre shortening matters because fibre length partly governs the mechanical response of fibrous materials [4]. To meet minimum property requirements, products made from recycled fibres generally require strengthening agents or the addition of virgin fibres [5]. Recycled fibres also tend to be channelled into low-grade products such as packaging paper, paperboard, and tissue [2]. A similar situation exists in engineering. Natural fibres and recycled materials are studied as low-cost green materials, yet their performance does not always match that of conventional materials [6]. The problem is therefore global: recycled fibres are valued more for their availability than for their performance. Strength also matters in printing. Gregersen [7] reported that fracture toughness, tensile strength and elongation at

break appear to correlate negatively with the break rate [7]. Linking web break statistics directly to paper properties could help to improve the mechanical performance of fibrous materials such as paper. Increasing the strength of recycled paper without virgin fibres or additives could therefore widen its use, potentially including printing grades.

The weakening of recycled fibres is rooted mainly in hornification, the largely irreversible closure of the cell wall structure caused by drying. Hornification reduces the swelling capacity of fibres, decreases their flexibility, and weakens their inter-fibre bonding potential [2], [8]. Sellman et al. [8] described hornification as a kinetically trapped state. Mo et al. [9] proposed cellulose recrystallisation during thermal drying as the main mechanism. Mo et al [10] reported that five recycling cycles reduced the relative bonded area of eucalyptus fibres by 17.6%, whereas the relative bonding force decreased by only 1.8%. This indicates that the main damage occurs in the inter-fibre contact area. Remedial efforts to date have operated at the fibre or bond level. Enzymatic refining can save up to ~20% of energy but still requires additional mechanical refining [11]. High-shear homogenisation increases tensile strength without impairing drainage [12]. Li et al. [13] reported that modified nanocellulose additives raised the tensile index of recycled paper by ~32%. The addition of virgin fibres or nanocellulose also improves the mechanical properties of recycled paper [5]. However, all these solutions modify only the fibres or their bonds. None of them changes the network architecture, that is, the way in which fibres are arranged within the sheet plane.

Network architecture, particularly fibre alignment, has long been recognised as a design parameter in the mechanics of fibrous materials. Fibre network models show that the effective stiffness of a sheet in the dominant direction increases as the Cox orientation distribution function becomes more anisotropic [14]. Micro-computed tomography (micro-CT) studies also confirm that fibre alignment is an essential input for mechanical models of paper and paperboard [15]. The same principle applies to composites. Ply orientation significantly affects the free vibration response of laminated plates [16]. The type and weight of the reinforcing fibres also contribute to the buckling load of cross-ply plates [17]. Rearranging recycled discontinuous fibres has even become an established strategy for restoring performance. Hecker et al. [18] realigned carbon fibres reclaimed from end-of-life sails. Balaga et al. [19] reported that randomly oriented recycled carbon fibre preforms reach only ~20% of the strength of equivalent continuous fibre composites. In contrast, aligned versions achieve full modulus translation. Other recycled fibres can likewise approach the performance of virgin fibres when used appropriately. Alignment therefore has the potential to add value to recycled cellulose fibres without relying on improvements in the quality of the fibres themselves.

Wet-state alignment has been investigated in several cellulose systems. Aligned cellulose nanofibril films have been produced by hydrogel stretching and wet spinning [20]. For bacterial cellulose, post-harvest hydrogel stretching has been widely studied. Saadi et al. [21] showed that in situ nanofibril alignment during biosynthesis increased tensile strength by ~137% compared with randomly oriented sheets. For wood pulp, the picture is more complex. Kouko et al. [22] strained paper webs during wet pressing and drying. Straining raised the tensile stiffness of the dried paper and reduced its strain at break[22]. Paper stiffness is also affected by internal drying stresses [15]. The alignment estimated from mechanical tests may therefore deviate from the actual fibre alignment. Drying stresses even alter individual fibres. Vonk et al. [23] showed that fibres from restrained-dried sheets exhibit a much smaller longitudinal hygro-expansion than freely dried fibres. This difference is consistent with sheet-scale behaviour. Network alignment effects and fibre-level effects are therefore intertwined. It is unclear whether wet straining (WS) can align hornified recycled fibres, because hornification reduces their swelling capacity and flexibility. Separating the contribution of alignment from fibre-level effects requires a route that changes the fibre orientation without changing the fibres or adding material.

Fibre orientation is an established design parameter for engineering materials, from laminated composite plates [16], [17] to composites made from recycled carbon fibres [18], [19]. Natural and recycled fibres are attractive as low-cost green engineering materials, but their use is often limited by their lower performance [6]. Recycled cellulose fibres face the same limitation, which alignment could address without additional material. This study aimed to examine fibre alignment through wet straining as a strategy for increasing the strength of recycled paper. It also aimed to compare the stiffness, tensile strength and fracture resistance of strained sheets tested along and across the straining direction with those of unstrained sheets. Wet sheets were formed from used paper without virgin fibres or chemical additives. The sheets were strained in tension at a low strain rate while still wet. Hot pressing then dried and consolidated them. Furthermore, tensile properties were measured at 0° and 90° to the straining direction, with randomly oriented sheets as the control. Fracture resistance was measured by single-edge-notched tension (SENT) tests. This concept could provide a route to recycled paper with higher tensile strength and fracture resistance along the straining direction, with potential relevance to printing. It could also transfer to other fibre networks with similar wet-state mobility, from macrofibres to nanofibrils, and support the circular use of recycled fibrous materials in engineering applications.

2 Materials and methods

2.1 Material

Used paper was the raw material for the recycled paper. It consisted of A4 sheets measuring 210 × 297 mm with a grammage of 100 g m−2. The paper was collected and manually inspected to remove staples, metal parts, and other contaminants before processing. Pretreatment consisted of soaking in mains water for 8 h. The water was used as received without further purification. No virgin fibres, reinforcing agents, or chemical additives were added. The differences between the sample groups can therefore be attributed to the straining treatment and the test direction.

2.2 Manufacturing (aligned) recycled papers

Recycled paper was manufactured from used paper in five sequential steps: soaking, disintegration, vacuum filtration, wet straining and hot pressing (Figure 1). The process started with soaking the used paper (Section 2.1). This helped to release the ink, stabilise the pH and soften the fibre network, which facilitated disintegration. Used paper with a dry mass of 9.5 g, weighed before soaking, was dispersed in water. Back-calculated from the grammage of the formed sheets, assuming complete fibre retention, the fibre consistency was ~2.4% (~380 g of water). To obtain a homogeneous fibre suspension, this mixture was disintegrated in a kitchen blender (Cosmos, Indonesia) at 3500 rpm for 5 min. The pH of the suspension was measured with a calibrated digital pH meter and adjusted to neutral (pH ~7.0). A portion of the suspension (47.5 g, wet mass) was then vacuum filtered in a ceramic Buchner funnel (110 mm in diameter; nominal sheet-forming area ~95 cm²) lined with type 103 slow-speed filter paper (pore size 15 µm). After 10 min, a circular wet fibre sheet had formed. To align the fibres, the semi-wet sheet was peeled off the filter paper after vacuum filtration and clamped without the filter paper in a universal testing machine (JTM UTS510l, Taiwan). It was then strained uniaxially at a crosshead speed of 1 mm min−1 to a strain of 3.6%, calculated from the crosshead displacement (~1.98 mm) divided by the initial grip distance of 55 mm. The fibres remain mobile in the wet state. At this low straining rate, the fibres are expected to reorient along the loading direction. Finally, the strained sheet was released from the grips and immediately transferred to a hydraulic hot press, where it was dried and consolidated at 0.69 MPa and 120 °C for 10 min to lock in the fibre orientation. The applied strain was not maintained mechanically during the transfer; the platen pressure restrained the sheet during drying. The pressure was monitored with an integrated manometer while a digital proportional–integral–derivative (PID) controller regulated the temperature. The result was a dry recycled paper sheet (Figure 1). Reference sheets were prepared by the same procedure without the straining step. Table 1 lists the sample groups.

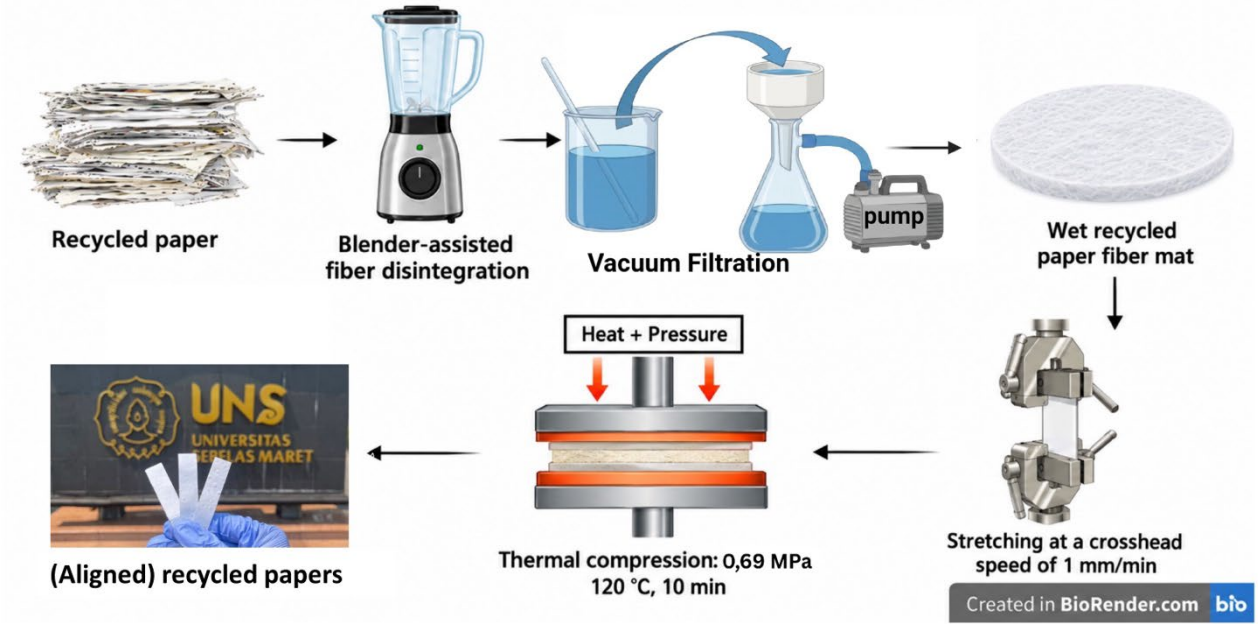

Fig. 1 Schematic of sample preparation: fibre disintegration in a blender, suspension preparation, vacuum filtration, wet-sheet formation, straining, hot pressing, and the final dry sheet

Table 1 Sample name and preparation treatments used in this study. The notation of alignment can be seen in Figure 2A

Sample name	Treatment
No straining	Hot pressed after wet laying, without straining
WS 0	Wet straining; loaded parallel (0°) to the straining direction in the tensile test
WS 90	Wet straining; loaded perpendicular (90°) to the straining direction in the tensile test

2.3 Characterisation of physical and mechanical properties of recycled papers

2.3.1 Grammage

Grammage, defined as the mass of a sheet per unit area, was determined in accordance with ISO 536. Specimens were weighed on a Joanlab FA2003s analytical balance with a readability of 0.001 g. The grammage was calculated using Equation (1) [24]:

$$\text{grammage} = \frac{m}{A} \times 10^6 \quad (1)$$

where grammage unit is g m^{-2}, m is the specimen mass (g), and A is the specimen area (mm^2).

2.3.2 Thickness

Sheet thickness was measured in accordance with ISO 534 using a Mitutoyo MDC-25PX micrometer with a resolution of 0.001 mm. Measurements were taken at three evenly distributed points on each specimen. The mean value was used to calculate the tensile stress.

2.3.3 Porosity and density

Bulk density (ρ_b, in g cm^{-3}) was calculated by dividing the specimen grammage (g m^{-2}) by the mean thickness (μm). Porosity was calculated using a true density of cellulose of 1.50 g cm^{-3} reported in previous research [25], according to Equation (2) [26]:

$$P(\%)=\left(1-\frac{\rho_b}{\rho_t}\right)\times 100 \quad (2)$$

where P is the porosity, ρ_b is the bulk density of the sheet, and ρ_t is the true density of cellulose. Five measurements were taken for each sample.

2.3.4 Morphology of cellulose fibres from used papers and recycled papers

The surface morphology of the cellulose fibres from used papers and of the recycled papers was characterised by scanning electron microscopy (SEM) using a JEOL JSM-6510LA microscope (JEOL Ltd., Tokyo, Japan). SEM images were acquired in secondary electron imaging (SEI) mode at an accelerating voltage of 20 kV, a working distance of 11 mm, and a magnification of 150×. These images were used to observe the fibre width, length and alignment. Fibre orientation was analysed using ImageJ on one SEM image per group. The ratio of the maximum value of the directionality histogram to the random level (~1.1%) was used as an orientation index.

2.3.5 Tension

Tensile tests were conducted with reference to ASTM D828-22 on a universal testing machine (Lixian HZ-1007A, Dongguan Lixian Instrument Scientific Co., Ltd, Dongguan City, China) equipped with a 50 kg load cell (resolution 0,00245 N). Before testing, the specimens were stored in sealed plastic bags containing silica gel and were then tested at ambient laboratory conditions (~26 °C, ~55% RH). Specimens measuring 15 mm × 75 mm were cut parallel (0°) and perpendicular (90°) to the straining direction (Figure 2A). The reference specimens were cut from sheets with random fibre orientation. Both ends of each specimen were mounted in a frame, giving a gauge length of 55 mm (Figure 2A). The tests were performed at a crosshead speed of 1 mm min−1 with five specimens per group. The span and crosshead speed deviated from ASTM D828-22 because of the limited size of the laboratory sheets and to match the rate used for wet straining and the SENT tests. Strain was calculated from the crosshead displacement divided by the gauge length. Because the crosshead displacement includes machine compliance, the modulus values are apparent and are used only to compare the groups. The forces measured (~8–30 N) were small relative to the load cell capacity, so all groups were tested with the same set-up.

2.3.6 Single-edge-notched tension (SENT)

The fracture toughness test was conducted using a rectangular single-edge-notched tension (SENT) specimen measuring 15 mm × 75 mm on the same machine used for the tensile test. An initial notch 4.0–4.5 mm long was made in the centre of one side of the specimen using a sharp scalpel, perpendicular to the direction of loading. The a/w ratio was therefore 0.27–0.30 [26]. The specimens were tested at a crosshead speed of 1 mm min−1, and five specimens were tested for each group. The fracture resistance was expressed as the apparent fracture toughness Kmax. Kmax was calculated from the maximum stress σmax reached during the test, not from the crack initiation load. It therefore reflects the resistance to crack propagation rather than to crack initiation. Linear elastic fracture mechanics (LEFM) requires large specimens and is strictly valid only for brittle paper grades [7]. Paper deforms non-linearly before failure, and the specimens in this study were only 15 mm wide. Kmax is therefore reported as an apparent value and is used only to compare groups tested with identical geometry and conditions. Kmax was calculated using Equation (3), and the geometric factor Y using Equation (4) [26].

$$K_{max},\ \text{MPa m}^{0.5}=\sigma_{max}Y\sqrt{a} \quad (3)$$

where σ_{max} is the maximum stress reached during the test and Y is:

$$Y=1.99-0.41\left(\frac{a}{w}\right)+18.7\left(\frac{a}{w}\right)^2-38.48\left(\frac{a}{w}\right)^3+53.85\left(\frac{a}{w}\right)^4 \quad (4)$$

where K_{max} is the apparent fracture toughness (MPa m$^{0.5}$), a is the initial crack length, w is the specimen width, and Y is the geometric factor.

2.3.7 Data analysis

The test data are described using means and 95% confidence intervals (CI). Differences among the three sample groups (No straining, WS 0, and WS 90) were evaluated using one-way analysis of variance (ANOVA) at a significance level of $\alpha = 0.05$. When ANOVA indicated a significant difference ($p < 0.05$), the analysis was followed by Tukey's honestly significant difference (HSD) multiple comparison test, which adjusts the p values for the number of pairwise comparisons. The Tukey test results are presented as a compact letter display (CLD). Groups sharing at least one letter do not differ significantly, whereas groups with different letters differ significantly ($p < 0.05$). The CLD

letters indicate the significance of the results for each sample group. Statistical analyses were performed using OriginPro 2026.

3 Results and discussion

3.1 Morphology of cellulose fibres from used papers

Fibre geometry affects network formation and load transfer in recycled paper. The cellulose fibres from used papers were therefore characterised first. Figure 2B shows the length distribution of the fibres obtained by mechanical disintegration in a blender. The mean fibre length was 787.7 ± 102.5 µm (mean ± standard deviation), with a unimodal distribution. About 68% of the fibres were 700–900 µm long. The mean fibre width was 25.55 ± 10.92 µm, giving a length-to-width ratio of ~30.8. The coefficient of variation of the width was 42.7%. This indicates that the transverse dimensions of the fibres are heterogeneous. This may be related to cross-sectional deformation, fibrillation and fragmentation during processing and recycling [1], [2]. In a sheet, the elongated fibres form crossings and inter-fibre contacts, which act as load-transfer paths. According to the tensile strength theory of paper developed by Page [35], the mechanical properties of a sheet depend not only on fibre length. They also depend on individual fibre strength and the effectiveness of inter-fibre bonding. The SEM image in Figure 2C shows the cellulose fibres from used papers. Their widths differ visibly, in line with the width variation described above. Fine fibrillar elements are visible on the fibre surfaces, consistent with the fibrillation mentioned above. All groups were prepared from the same pulp suspension. The initial fibre geometry should therefore be similar in all groups. Differences in mechanical response between groups are more appropriately analysed in relation to the arrangement of the fibres in the sheets after treatment (Section 3.2).

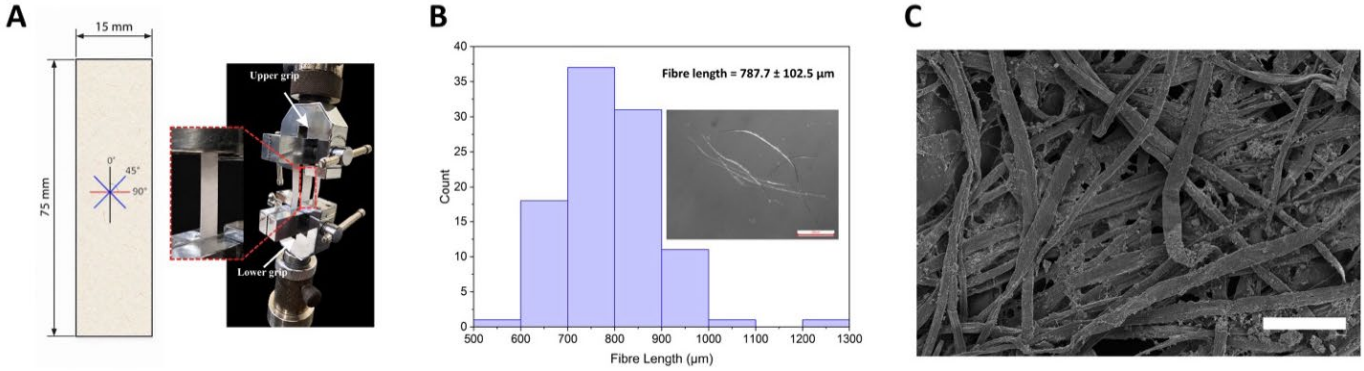

Fig. 2 (A) specimen schematic with the marked fibre orientations and the tensile test setup; (B) fibre length distribution (inset: micrograph of the fibres); (C) SEM image of the cellulose fibres from used papers. *Scale bar* = 200 µm

3.2 Morphology of recycled papers

Fibre orientation on the sheet surface was analysed in ImageJ using three approaches: vector analysis, colour mapping and directionality (Figure 3). In all images, the vertical axis corresponds to the tensile loading direction of the specimen. The vector analysis in Figure 3A shows the dominant fibre direction in each grid cell as a yellow line. In WS 0, most vectors were oriented close to the vertical axis. Only a few vectors were oblique. Almost none were close to the horizontal. In WS 90, most vectors were oriented close to the horizontal axis, nearly perpendicular to those of WS 0. This agrees with the experimental design, because WS 0 and WS 90 were cut from the same strained sheets at 90° to each other. In contrast, the vectors in No straining pointed in all directions and did not form a dominant direction. This suggests that the unstrained sheet had a random in-plane fibre network. A similar contrast has been reported for industrial paperboard. Specimens cut along the machine direction (MD) contain a larger proportion of fibres aligned with the load than those cut along the cross direction (CD) [28]. The vector analysis therefore suggests that wet straining rearranged the large fibres towards the straining direction. However, the vectors in WS 0 and WS 90 were not perfectly parallel. They deviated by ~20° from the image axes, indicating that the alignment was moderate rather than complete.

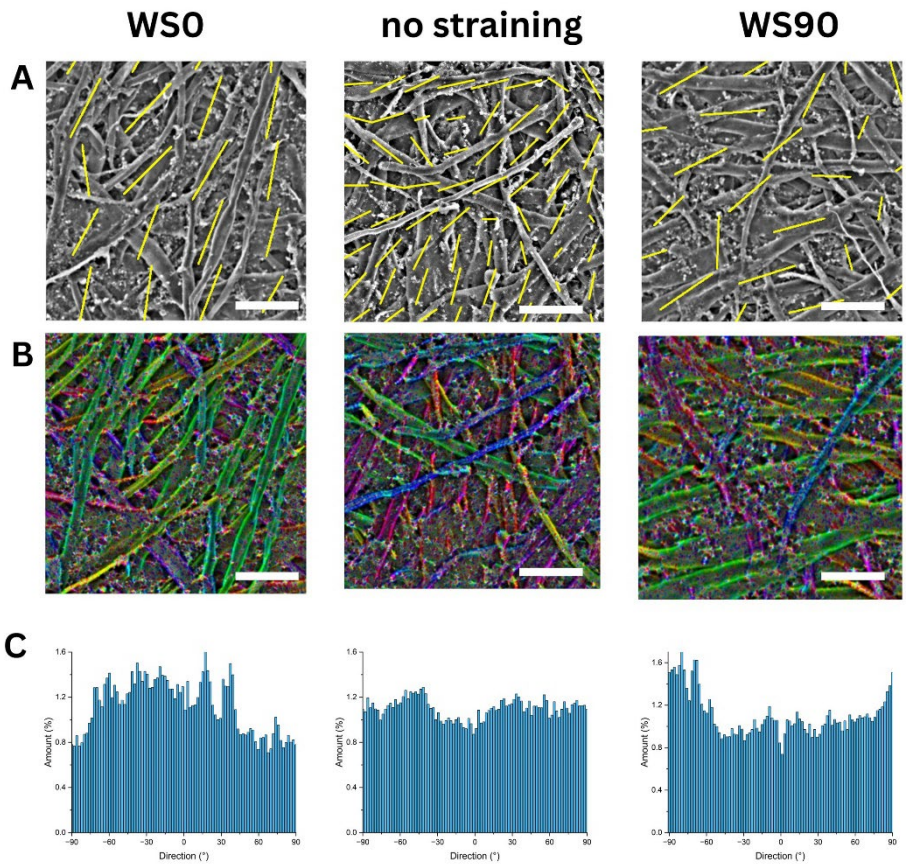

Fig. 3 Fibre orientation analysis of WS 0, No straining and WS 90 using ImageJ: (A) vector analysis; (B) orientation colour map; (C) directionality histogram. *Scale bar* = 100 µm (A and B)

The colour map in Figure 3B shows the local fibre orientation as colour hue. The brightness follows the original SEM image. Regions with a dominant orientation appear within a narrow hue range. Randomly oriented regions display the entire colour spectrum. In WS 0 and WS 90, the large fibres are dominated by a single hue group. This suggests that most fibres in each image have one dominant orientation. Other hues appear mainly in fine fibrils, fibre edges and the background between fibres. In contrast, No straining shows blue, magenta, red, yellow and green fibres in nearly equal proportions, without a dominant hue. This agrees with the random in-plane orientation seen in the vector analysis. The colour map also shows that the orientation in WS 0 and WS 90 is not uniform, because fibres with other hues still intersect the dominant fibre population. Gobes et al. [29] also reported a broad distribution of orientations and low coherence in laboratory sheets analysed with the *structure tensor* method. The colour map therefore supports the dominant directions found by the vector analysis.

Figure 3C shows the directionality histograms, which quantify the amount of structures at each angle. In this analysis, angles are referenced to the vertical axis of the image. A peak around 0° indicates vertically oriented fibres. A peak around ±90° indicates horizontally oriented fibres. A uniform distribution indicates random orientation. In a random distribution, each angular bin has a value of ~1.1%. WS 0 shows a broad plateau of elevated values between about −70° and +40°, centred near −15°, with local maxima of up to ~1.6%. The values decrease to ~0.8% towards ±90°. This indicates a dominant fibre orientation close to the vertical axis. WS 90 shows the opposite pattern. Its highest values, up to ~1.7%, lie between −90° and −65° and rise again near +90°. The smallest values occur around 0°. This indicates a predominance of horizontal fibres. No straining shows a nearly flat distribution at ~1.1% across the entire angular range, with only small local fluctuations. This is consistent with a random orientation of the unstrained network. However, the WS 0 and WS 90 histograms remain broad. Their orientation index was only ~1.5, compared with ~1.1 for no straining. Such broad distributions are characteristic of laboratory sheets, which are far less anisotropic than machine-made paper [29]. Overall, the three approaches consistently show that wet straining produced a dominant fibre direction parallel to the straining axis, with a moderate degree of orientation. According to Cox's theory, a moderate degree of orientation is expected to result in a mechanical anisotropy of similarly moderate magnitude [30].

3.3 Physical and mechanical properties of recycled papers

WS 0 had the highest density and grammage and the smallest porosity (Figure 4A). This trend is expected, because porosity was calculated from density (Equation 2). However, all three groups shared the same letter in the compact letter display (CLD) for every parameter. The grammage of all groups remained within 120.00–126.86 g m^{-2}. The porosity remained within 60.04–60.78%. Density, porosity and grammage therefore did not differ significantly among

the groups at the 5% significance level. This is also expected, because all sheets were formed from the same fibre suspension and press-dried under identical conditions. Wet straining presumably rearranged the fibre direction rather than compacting the network. The small differences between WS 0 and WS 90 should be interpreted with caution. Both groups were cut from sheets that received the same straining treatment and differed only in cutting direction. These differences therefore reflect local variation between specimens, not an effect of test direction. This similarity is relevant to the mechanical properties. Paper strength depends not only on density but also on the contact area and the effectiveness of inter-fibre bonding [31]. The three groups had a similar degree of densification. The differences in mechanical response are therefore unlikely to come from densification. They are more likely to come from changes in network architecture, particularly the fibre direction relative to the loading direction (Figure 3).

Figure 4B shows the tensile modulus and strength of our recycled paper. Wet straining improved the tensile properties along the straining direction. No straining exhibited a tensile modulus of only 0.36 GPa (AB) and a tensile strength of 8.34 MPa (ab). When loaded along the straining direction, the tensile modulus of WS 0 increased by 142% to 0.87 GPa (C). Its tensile strength increased by 22% to 10.15 MPa (c). Loading perpendicular to the straining direction gave lower mean values for WS 90, with a tensile modulus of 0.223 GPa (A) and a tensile strength of 5.43 MPa (a). However, these values did not differ significantly from those of No straining.The letters C and c show that WS 0 differed significantly from the other two groups in both properties. No straining shared the letters A and a with WS 90, indicating that the two groups did not differ significantly. This directional behaviour can be attributed to the fibre orientation relative to the loading direction, which governs the stiffness and strength of a fibre network [30]. Fibres aligned with the load carry it axially. Inclined fibres must first rotate and deform their bonds before contributing to load transfer. The tensile load acted along the specimen axis in all groups. Fibres that were not aligned with this axis may therefore have reoriented towards the loading direction during the test. This may have happened in both No straining and WS 90, which contained many such fibres (Figure 3). The reorientation may have reduced the initial difference in fibre direction between the two groups. It could therefore explain why they did not differ significantly. In WS 0, the same reorientation may have added to the alignment produced by wet straining. This could have raised the tensile modulus and tensile strength of WS 0 further. Wet straining affected the tensile modulus more strongly than the tensile strength. This agrees with Seth and Page [27]. They showed that the deformation of paper is governed mainly by the fibres. Bonding largely determines the point of failure.

To exclude the effect of sheet density, we also evaluated the specific modulus and tensile index of our recycled paper (Figure 4C). The specific modulus of WS 0 increased by 136% to 1.44 kN m g^{-1} (C) compared with No straining (0.61 kN m g^{-1}, AB). WS 90 had a lower mean specific modulus of 0.38 kN m g−1 (A). The tensile index of WS 0 reached 17.12 N m g^{-1} (c), an increase of 22% over No straining (14.06 N m g^{-1}, ab). WS 90 had a lower mean tensile index of 9.15 N m g−1 (a); neither value differed significantly from No straining. As for the tensile properties, WS 0 differed significantly from the other two groups, which shared the same letter. These results suggest that the improvement in WS 0 comes from a more efficient use of the fibres, not from a larger amount of material. Oriented cellulose fibre materials are known to exploit the intrinsic stiffness and strength of the fibres most efficiently along the orientation direction [32].

We also investigated the fracture resistance of our recycled paper using the SENT test (Figure 4D). No straining had a K_{max} of 0.83 MPa $m^{0.5}$ (ab). WS 0 had the highest K_{max} of 1.51 MPa $m^{0.5}$ (c). WS 90 had the smallest K_{max} of 0.53 MPa $m^{0.5}$ (a). WS 0 differed significantly from both No straining and WS 90 in K_{max}. No straining and WS 90 did not differ significantly. Compared with No straining, WS 0 had an 82% higher K_{max}. The higher K_{max} of WS 0 is discussed below with the SENT curves. Nevertheless, the fracture toughness of our recycled paper is smaller than that of cellulose nanopaper [25]. This is probably due to the larger fibre size and the weaker bonding of hornified recycled fibres.

Figure 5A shows the representative tensile stress–strain curves of our recycled paper. All groups exhibited the bilinear response typical of cellulose fibre networks. The initial linear region is governed by the elastic deformation of fibres and inter-fibre bonds. The knee point marks the onset of fibre plasticity and progressive bond failure [33], [28]. Beyond the knee point, fibre straightening further contributes to network elongation [34]. Wet straining kept the bilinear shape of the curves but shifted the stress level at every stage of deformation. WS 0 reached the knee point at ~8 MPa and ~0.5% strain. No straining and WS 90 reached it at only ~5 MPa and ~3.5 MPa, respectively, both at ~0.7% strain. The stiff and strong response of WS 0 resembles the MD of industrial paper. The more compliant response of WS 90 resembles the CD [28]. It is worth mentioning that the strain at break did not differ significantly between the groups. It was 3.28 ± 0.80%, 2.69 ± 0.58% and 2.60 ± 0.49% (mean ± 95% CI) for WS 0, No straining and WS 90, respectively. Since all sheets were dried under restraint in the hot press, free shrinkage of the strained sheets was prevented. Restrained drying limits the microcompressions formed in fibres during drying shrinkage [27]. It also alters the fibre and sheet behaviour compared with free drying [23]. The anisotropy measured mechanically may therefore differ from the actual fibre orientation [15].

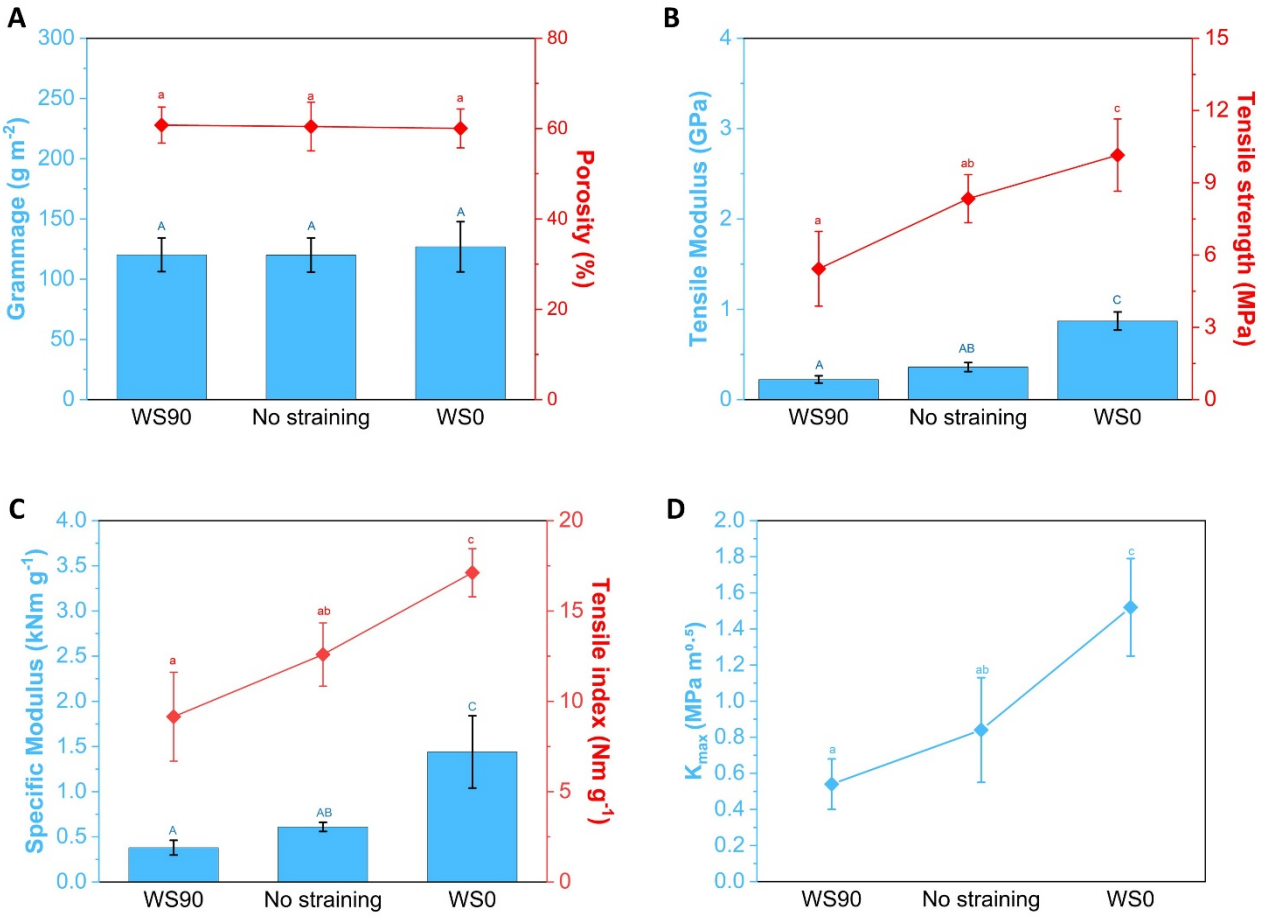

Fig. 4 Physical and mechanical properties of recycled papers: (A) grammage and porosity; (B) tensile modulus and tensile strength; (C) specific modulus and tensile index compared with reported tensile index values of recycled paper; and (D) K_{max}. Capital letters refer to the bars (left axis) and small letters to the symbols (right axis). Groups sharing a letter do not differ significantly. Error bars show the 95% CI (n = 5)

The SENT load–displacement curves (Figure 5B) reveal a clearer difference in fracture behaviour between the groups. All specimens exhibited crack initiation at the notch tip at a similar load of ~8–9 N. The differences in Kmax (Figure 4D) therefore arise after initiation, from the resistance to crack propagation. This suggests that crack initiation is governed by the inter-fibre bond network. The porosity of the three groups was similar (Figure 4A). After initiation, the load of WS 0 continued to rise to 31 N before abrupt failure at a displacement of 0.9 mm. No straining showed a load plateau of ~9 N between 0.2 and 0.4 mm, followed by a second rise to 19 N. In contrast, the load of WS 90 peaked at only 9 N and decreased gradually until failure at 0.6 mm. The rising load after crack initiation is probably caused by fibres bridging the crack. In WS 0, the notch was perpendicular to the dominant fibre direction. The crack therefore had to break or pull out the fibres lying across its path. In WS 90, the notch was parallel to the fibres. The crack could therefore propagate between the fibres through bond failure. Johansson et al. [28] also observed that the deformation and failure of paperboard differ between specimens loaded along and across the dominant fibre direction. The tensile load in the SENT test may also have reoriented fibres near the notch tip towards the loading direction. This may have happened in both No straining and WS 90. Some fibres may then have crossed the crack path in each group. This could explain why the K_{max} of the two groups did not differ significantly (Figure 4D). In WS 0, the same effect may have added to the fibre bridging described above.

Figure 5C compares the tensile index of our recycled paper with values reported for recycled and hornified pulp handsheets that received additional processing. Sheikhi et al. [36] formed handsheets from industrial OCC pulp, either alone (17.90 N m g−1) or blended with 10% virgin bagasse pulp that had been soda-cooked with 15% NaOH and refined in a valley beater (18.40 N m g−1). Giacomozzi and Joutsimo [37] used an industrial oxygen-delignified, ECF-bleached *Pinus radiata* kraft pulp that was oven-dried at 50 and 90 °C to induce hornification and tested unrefined (17.2 and 17.3 N m g−1). Li et al. [13] soaked OCC for 24 h, refined it to 37 °SR and added 0.3% nanocellulose grafted with DTPA and chitosan (19.47 N m g−1). In contrast, our sheets were made from used office paper alone, only soaked and disintegrated in a blender, without virgin fibres, refining, bleaching or chemicals. Wet straining and hot pressing nevertheless raised the tensile index of WS 0 to 17.12 N m g−1. This value is comparable with those of Giacomozzi and Joutsimo and of the unblended OCC sheets of Sheikhi et al. [36] , and only 7–12% below the bagasse-blended and nanocellulose-treated sheets, although WS 0 was loaded along the dominant fibre direction whereas the reference handsheets are nominally isotropic. WS 0 remains well below the tensile index typical

of printing and writing papers (40–45 N m g−1) [38]. Its relevance to printing grades is therefore potential, and combining wet straining with refining or strength additives is recommended for future work.

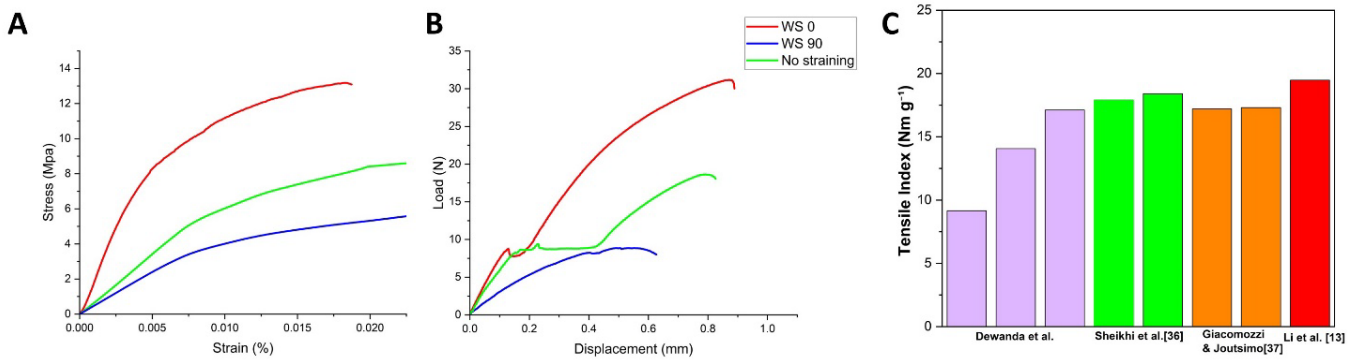

Fig. 5 (A) representative tensile stress–strain curves and (B) SENT load–displacement curves of the recycled papers (C) comparison of the tensile index of our recycled paper with that of handsheets that have undergone additional processing

4 Conclusions

Wet straining oriented the fibres of hornified recycled paper to a moderate degree without virgin fibres or chemical additives. WS 0 differed significantly from both No straining and WS 90 in tensile modulus, tensile strength and apparent fracture toughness. WS 90 did not differ significantly from No straining in any of these properties. This directional response can be attributed to the orientation of the fibres relative to the loading direction rather than to densification. The differences persisted after normalisation by density and grammage. The specific modulus and tensile index of WS 0 were 136% and 22% higher than those of no straining. This suggested a more efficient use of the fibres rather than a larger amount of material. In the SENT test, the load of WS 0 kept rising after crack initiation. This was probably caused by fibres bridging the crack, as the notch was perpendicular to the dominant fibre direction. The strain at break did not differ significantly among the groups. However, wet straining and restrained drying may also have changed the fibre and bond properties, so the measured differences cannot be attributed to fibre alignment alone. In addition, orientation was quantified from one SEM image per group. Tensile strength and fracture resistance are potentially relevant to the runnability of printing paper. Wet strength, which is also relevant to printing, was not tested and is recommended for future work. The tensile index of WS 0 was comparable with that of unreinforced recycled handsheets reported in the literature. Compliance with printing-grade requirements was not assessed. From an engineering perspective, fibre orientation can thus serve as a design parameter to tailor the mechanical properties of recycled fibrous materials without virgin fibres or additives, supporting the circular use of secondary fibres that are otherwise often downgraded to low-grade products.

5 Acknowledgements

This study received funding from Sebelas Maret University through the Master's Degree Graduate Research (PPSM) program under contract No. 460/UN27.22/PT.01.03/2026. The authors gratefully acknowledge the Department of Mechanical Engineering at Universitas Sebelas Maret and BRIN for access to its laboratory facilities. The authors thank Farras, Ahnaf, Adib, and Haikal for their assistance throughout the research.

6 References

[1] Parastar, M., Nazarnezhad, N., & Asadpour, Q. (2026). The effect of OCC fibers surface modification and polyvinyl alcohol on the properties of test liner paper. *BioResources, 21*(1), 341–357. https://doi.org/10.15376/biores.21.1.341-357

[2] Pătrăucean-Patrașcu, C. I., Gavrilescu, D.-A., & Gavrilescu, M. (2025). Chemical transformations and papermaking potential of recycled secondary cellulose fibers for circular sustainability. *Applied Sciences, 15*(24), Article 13034. https://doi.org/10.3390/app152413034

[3] Li, Y., Zambrano, F., Wang, Y., & Marquez, R. (2022). How China's foreign waste ban will reshape the U.S. recycling supply chain: Economic and environmental considerations towards a circular economy oriented paper recycling industry. *BioResources, 17*(2), 3178–3201. https://doi.org/10.15376/biores.17.2.3178-3201

[4] Singh, R., Nayak, S., Hegde, S., & Padmaraj, N. H. (2023). Influence of fiber length and moisture content on sound and vibration characteristics of hemp/epoxy composites. *Journal of Applied Engineering Science, 21*(3), 957–962. https://doi.org/10.5937/jaes0-44872

[5] Filipova, I., Andze, L., Skute, M., Zoldners, J., Irbe, I., & Dabolina, I. (2023). Improving recycled paper materials through the incorporation of hemp, wood virgin cellulose fibers, and nanofibers. *Fibers, 11*(12), Article 101. https://doi.org/10.3390/fib11120101

[6] Šupić, S., Poletanović, B., Radonjanin, V., Malešev, M., Merta, I., & Pantić, V. (2024). Influence of accelerated ageing on pull-off strength of concrete produced with recycled concrete aggregate and blended with hemp fibers. *Journal of Applied Engineering Science, 22*(2), 285–290. https://doi.org/10.5937/jaes0-50466

[7] Gregersen, Ø. W. (2005). Review: Runnability, fracture and pressroom breaks. In S. J. l'Anson (Ed.), Transactions of the XIIIth *Fundamental Research Symposium* (pp. 797–825). Fundamental Research Committee. https://doi.org/10.15376/frc.2005.2.797

[8] Sellman, F. A., Benselfelt, T., Larsson, P. T., & Wågberg, L. (2023). Hornification of cellulose-rich materials – A kinetically trapped state. *Carbohydrate Polymers, 318*, Article 121132. https://doi.org/10.1016/j.carbpol.2023.121132

[9] Mo, W., Chen, K., Yang, X., Kong, F., Liu, J., & Li, B. (2022). Elucidating the hornification mechanism of cellulosic fibers during the process of thermal drying. *Carbohydrate Polymers, 289,* Article 119434. https://doi.org/10.1016/j.carbpol.2022.119434

[10] Mo, W., Li, B., & Chen, K. (2024). The role of hornification in the deterioration mechanism of physical properties of unrefined eucalyptus fibers during paper recycling. *TAPPI Journal, 23*(2), 97–112. https://doi.org/10.32964/TJ23.2.97

[11] Rossi, C., & Solé, A. (2025). A systematic review on enzymatic refining of recycled fibers: A potential to be unlocked. *BioResources, 20*(3), 7870–7889. https://doi.org/10.15376/biores.20.3.Rossi

[12] Debnath, M., Salem, K. S., Musten, E., Lucian, L., Hubbe, M. A., & Pal, L. (2025). Renovating recycled fibres using high-shear homogenization for sustainable packaging and other bioproducts. *Packaging Technology and Science, 38*(4), 323–332. https://doi.org/10.1002/pts.2873

[13] Li, A., Xu, D., Zhang, M., Wu, S., Li, Y., Sun, W., Zhou, Y., Abo Madyan, O., Fan, M., & Rao, J. (2022). Grafting nanocellulose with diethylenetriaminepentaacetic acid and chitosan as additive for enhancing recycled OCC pulp fibres. *Cellulose, 29(*3), 2017–2032. https://doi.org/10.1007/s10570-021-04390-9

[14] Samantray, P., Peerlings, R. H. J., Massart, T. J., Rokoš, O., & Geers, M. G. D. (2022). Role of inter-fibre bonds and their influence on sheet scale behaviour of paper fibre networks. *International Journal of Solids and Structures, 256,* Article 111990. https://doi.org/10.1016/j.ijsolstr.2022.111990

[15] Kloppenburg, G., Li, X., Dinkelmann, A., Finckh, H., Neumann, J., & Simon, J.-W. (2024). Functional description of fiber orientation in paperboard based on orientation tensors resulting from µ-CT scans. *Cellulose, 31*(13), 7865–7893. https://doi.org/10.1007/s10570-024-06094-2

[16] Bojović, V., & Rakočević, M. (2024). Analytical and numerical solution for free vibrations of laminated composite plates. *Journal of Applied Engineering Science, 22*(2), 245–252. https://doi.org/10.5937/jaes0-50407

[17] Aljibori, H. S. S., Alhabeeb, S. A., Algelal, H. M. A., Asim, W. M. H., & Chong, W. P. (2023). Comparative study of cross-ply laminated composite materials and effect of buckling response with and without cutouts. *Journal of Applied Engineering Science, 21*(1), 45–58. https://doi.org/10.5937/jaes0-37990

[18] Hecker, M. D., Longana, M. L., Eloi, J. C., Thomsen, O., & Hamerton, I. (2023). Recycling end-of-life sails by carbon fibre reclamation and composite remanufacture using the HiPerDiF fibre alignment technology. Composites Part A: *Applied Science and Manufacturing, 173,* Article 107651. https://doi.org/10.1016/j.compositesa.2023.107651

[19] Balaga, U. K., Gunes, A., Ozdemir, T., Blackwell, C., Davis, M., Sauerbrunn, S., Fuessel, L., Deitzel, J. M., & Heider, D. (2025). Optimization of the recycling process for aligned short carbon fiber TuFF composites. *Recycling, 10*(2), Article 55. https://doi.org/10.3390/recycling10020055

[20] Daghigh Shirazi, H., Håkansson, K. M. O., Abitbol, T., & Vapaavuori, J. (2024). A facile spinning approach towards the continuous production of aligned nanocellulose films. Colloids and Surfaces *A: Physicochemical and Engineering Aspects, 701,* Article 134673. https://doi.org/10.1016/j.colsurfa.2024.134673

[21] Saadi, M. A. S. R., Cui, Y., Bhakta, S. P., Hassan, S., Harikrishnan, V., Siqueira, I. R., Pasquali, M., Bennett, M., Ajayan, P. M., & Rahman, M. M. (2025). Flow-induced 2D nanomaterials intercalated aligned bacterial cellulose. *Nature Communications, 16,* Article 5825. https://doi.org/10.1038/s41467-025-60242-1

[22] Kouko, J., Retulainen, E., & Kekko, P. (2014). Influence of straining during wet pressing and drying on strength properties of paper. *Nordic Pulp & Paper Research Journal, 29(*3), 453–461. https://doi.org/10.3183/npprj-2014-29-03-p453-461

[23] Vonk, N., Peerlings, R., Geers, M., & Hoefnagels, J. (2023). Effect of restrained versus free drying on hygro-expansion of hardwood and softwood fibers and paper handsheet. *Cellulose, 30*(17), 11135–11156. https://doi.org/10.1007/s10570-023-05473-5

[24] Villanueva-Linares, A. T., Aguilar-Franco, J. A., Chambi-Peralta, M. M., Rivera Calcina, C. R., Donaires Flores, T., & Díaz-Quintanilla, J. F. (2026). Physical, mechanical and chemical characterization of a composite from leather shavings and scrap office paper for potential packaging application. *Cleaner Waste Systems, 13,* Article 100469. https://doi.org/10.1016/j.clwas.2026.100469

[25] Henriksson, M., Berglund, L. A., Isaksson, P., Lindström, T., & Nishino, T. (2008). Cellulose nanopaper structures of high toughness. *Biomacromolecules, 9*(6), 1579–1585. https://doi.org/10.1021/bm800038n

[26] Wloch, D., Herrera, N., & Lee, K.-Y. (2023). Optically transparent laminated acrylic composites reinforced with mercerised bacterial cellulose nanopaper. Composites Part A: *Applied Science and Manufacturing, 172*, Article 107583. https://doi.org/10.1016/j.compositesa.2023.107583

[27] Seth, R. S., & Page, D. H. (1981). The stress strain curve of paper. In *Transactions of the VIIth Fundamental Research Symposium* (pp. 421–452). Fundamental Research Committee. https://doi.org/10.15376/frc.1981.1.421

[28] Johansson, S., Engqvist, J., Tryding, J., & Hall, S. A. (2021). 3D strain field evolution and failure mechanisms in anisotropic paperboard. *Experimental Mechanics, 61*(3), 581–608. https://doi.org/10.1007/s11340-020-00681-7

[29] Gobes, E. E., Wade, K., Gray-Stuart, E., Parker, K., & Bronlund, J. (2026). Characterising fibre alignment in moulded fibre materials across X, Y, and Z axes. *Cellulose, 33*(11), 6479–6496. https://doi.org/10.1007/s10570-026-07179-w

[30] Cox, H. L. (1952). The elasticity and strength of paper and other fibrous materials. *British Journal of Applied Physics, 3*(3), 72–79. https://doi.org/10.1088/0508-3443/3/3/302

[31] Schmied, F. J., Teichert, C., Kappel, L., Hirn, U., Bauer, W., & Schennach, R. (2013). What holds paper together: Nanometre scale exploration of bonding between paper fibres. *Scientific Reports, 3*, Article 2432. https://doi.org/10.1038/srep02432

[32] Jakob, M., Mahendran, A. R., Gindl-Altmutter, W., Bliem, P., Konnerth, J., Müller, U., & Veigel, S. (2022). The strength and stiffness of oriented wood and cellulose-fibre materials: A review. *Progress in Materials Science, 125*, Article 100916. https://doi.org/10.1016/j.pmatsci.2021.100916

[33] Baumann, G., Czibula, C., & Hirn, U. (2025). The tensile behaviour of paper under high loading rates. *Cellulose, 32*(2), 1201–1219. https://doi.org/10.1007/s10570-024-06266-0

[34] Wu, D., Engqvist, J., Barbier, C., Karlsson, C., & Hall, S. (2022). Unravelling the deformation process of a compacted paper: In-situ tensile loading, 4D X-ray tomography and image-based analysis. *International Journal of Solids and Structures, 242*, Article 111539. https://doi.org/10.1016/j.ijsolstr.2022.111539

[35] Page, D. H. (1969). A theory for the tensile strength of paper. *TAPPI Journal, 52*(4), 674–681.

[36] Sheikhi, P., Asadpour, G., Zabihzadeh, S. M., & Amoee, N. (2013). An optimum mixture of virgin bagasse pulp and recycled pulp (OCC) for manufacturing fluting paper. *BioResources, 8*(4), 5871–5883. https://doi.org/10.15376/biores.8.4.5871-5883

[37] Giacomozzi, D. E., & Joutsimo, O. (2015). Drying temperature and hornification of industrial never-dried Pinus radiata pulps. 1. Strength, optical, and water holding properties. *BioResources, 10*(3), 5791–5808. https://doi.org/10.15376/biores.10.3.5791-5808

[38] González, I., Boufi, S., Pèlach, M. A., Alcalà, M., Vilaseca, F., & Mutjé, P. (2012). Nanofibrillated cellulose as paper additive in eucalyptus pulps. *BioResources, 7*(4), 5167–5180. https://doi.org/10.15376/biores.7.4.5167-5180ol. 7, no. 4, pp. 5167–5180, 2012, doi: 10.15376/biores.7.4.5167-5180

7 Conflict of interest statement

The authors declare that they have no conflicts of interest.

8 Author contributions

Gigih: Conducted the experiments, processed and analysed the data, and drafted the manuscript. Ubaidillah: Reviewed the manuscript and provided revisions and feedback. Azahra: Facilitated the SEM characterisation. Joanne Li: Assisted with data visualisation. Mujtahid: Facilitated the universal testing machine. Dharu: Developed the manuscript outline and organised its structure.

9 Availability statement

All relevant data are included within the article.

10 Supplementary materials

No supplementary materials accompany this article

Paper submitted: 29.09.2026.
Paper accepted: 12.11.2026.
This is an open access article distributed under the CC BY 4.0 terms and conditions